Molecular Dynamics Simulations of Isolated Helices of Myoglobin†

Jonathan D. Hirst and Charles L. Brooks III*

Department of Molecular Biology, The Scripps Research Institute, 10666 North Torrey Pines Road, La Jolla, California 92037

Received December 22, 1994; Revised Manuscript Received April 12, 1995⊗

ABSTRACT: The apo form of myoglobin has two non-native stable states that have been experimentally characterized. Investigation of these states has suggested possible folding pathways for myoglobin. We have performed molecular dynamics simulations on solvated isolated helices of myoglobin to investigate the relationship between the intrinsic stabilities of the isolated helices and the structure and folding pathway of apomyoglobin. Analyses of hydrogen bonding and fluctuations from simulations at 298 and 368 K are used to explore the relative stabilities of the helices of myoglobin. The ordering observed is A ≈ G ≈ H > B > E > F, which mirrors both the experimental equilibrium and kinetic data available for apomyoglobin. The experimental observation that a subdomain comprising helices A, G, and H is an important early intermediate and our result that these helices are the most stable suggest that the intrinsically more stable helices form early in the folding process and that this significantly influences the folding pathway.

The protein folding problem—understanding how the sequence of a protein is related to its three-dimensional structure—is the subject of numerous different approaches (Creighton, 1992). Due to the rapid and generally highly cooperative nature of the protein folding process, the experimental characterization of folding intermediates is difficult and much remains to be understood about protein folding pathways. Two strategies that have provided useful experimental data on potential folding intermediates are the characterization of apoproteins (Hughson et al., 1990; Barrick & Baldwin, 1993) and the study of peptides (Dyson et al., 1992a,b). Both these strategies have been employed to investigate the folding of myoglobin, an extensively studied paradigm of protein folding. We relate the molecular dynamics simulations presented here to the available experimental data on apomyoglobin and on isolated helical peptide fragments from myoglobin.

Myoglobin is a globular, heme protein, with 153 residues, and comprises eight α-helices (see Figure 1). There has been extensive experimental characterization of apomyoglobin and its folding pathway (Hughson et al., 1990; Jennings & Wright, 1993), although there is no X-ray crystal structure. Two non-native apo states have been studied by site-directed mutagenesis, H/^{2}H labeling, and CD experiments (Hughson et al., 1990; Barrick & Baldwin, 1993): (1) a compact globule, with about 60% of native secondary structure at 278 K and neutral pH, as suggested by a 40% reduction in the measured CD at 222 nm; (2) the I state, which exists at 278 K and pH 4 and has only 35% of the native secondary structure. Hydrogen-exchange pulse labeling and stopped-flow CD experiments by Jennings and Wright (1993) indicate that the structure of the earliest detectable intermediate formed during refolding of apomyoglobin is very similar to the I state. Privalov and co-workers (Griko et al., 1988; Griko & Privalov, 1994) have studied the thermodynamics of the unfolding of apomyoglobin. The acid denaturation of apomyoglobin (Barrick et al., 1994; Yang & Honig, 1994) and also the cold denaturation (Nishii et al., 1994) have been investigated. The structural and thermodynamic properties of the apoprotein under native conditions provide an otherwise inaccessible description of a possible folding intermediate (Cocco et al., 1992).

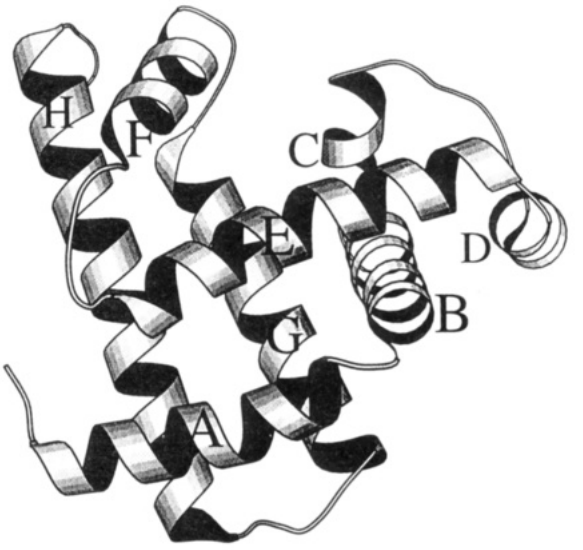

FIGURE 1: Structure of myoglobin, depicted using MOLSCRIPT (Kraulis, 1991). The eight helices are labeled A−H.

Peptide fragments of proteins have provided experimental models to investigate the earliest events in protein folding. To identify transient structures that might be important early in the folding of apomyoglobin, Wright and co-workers have characterized peptide models corresponding to helical fragments G and H of myoglobin using CD and NMR (Waltho et al., 1989, 1993; Shin et al., 1993a,b). These studies found the H-helix fragment to be 30% helical as determined by CD (Waltho et al., 1993). NMR experiments (Waltho et al., 1989) indicate that the C-terminal fragment of helix H [residues 132−153, as identified in the X-ray crystal structure of sperm whale myoglobin (Phillips, 1980)] has small, but significant, preferences for helical conformations. The

† Partially supported by NIH Grants GM 37554 and GM 48807. J.D.H. is supported by a long-term fellowship from the Human Frontiers Science Program.

* To whom correspondence should be addressed.

⊗ Abstract published in *Advance ACS Abstracts,* May 15, 1995.

0006-2960/95/0434-7614$09.00/0

N-terminal portion of helix H (residues 124−130) consists mainly of unfolded conformations (Waltho et al., 1993). The peptide fragment of helix G was not significantly helical in isolation, but helix formation was readily induced by the addition of trifluoroethanol, which is indicative of helical propensity (Shin et al., 1993b). It was concluded from this work that the peptides corresponding to helices G and H have high propensities for helix formation and that helix H, in particular, has a role in the early folding events.

Complementing the experimental work noted above, there have been molecular dynamics simulations of the apoprotein at pH 7 and at pH 4 and of the H-helix peptide region in isolation. Simulations of apomyoglobin under various conditions of pH and temperature suggest that helix F is unstable (Brooks, 1992; Tirado-Rives & Jorgensen, 1993). Soman et al. (1993) have examined the unfolding of the C-terminal fragment of helix H using molecular dynamics. They observed almost complete unfolding over a period of 1 ns. Various mechanisms of unfolding were identified, including the insertion of a water molecule in helical hydrogen bonds and unfolding via an $i, i + 3$ hydrogen bond.

We have extended earlier work of Soman et al. (1991) to look at six of the helices of myoglobin. In this work, we investigate the extent to which the intrinsic stability of individual helices is correlated with early events in the folding of apomyoglobin by performing molecular dynamics simulations of isolated helices from myoglobin. From these simulations, we estimate the relative stabilities of the helices; the use of identical protocols minimizes uncertainties inherent in the single simulation studies which have preceded ours. Regions of instability observed in the simulations allowed us to identify important tertiary interactions and to examine the pathways of unfolding transitions in helices.

METHODS

Simulations were performed on the following isolated helical peptide fragments of myoglobin: A (residues 3−18: SEGEWQLVLHVWAKVE), B (residues 20−35: DVAGHGQDILIRLFKS), E (residues 58−78: SEDLKKHGVTVLTALGAILKK), F (residues 86−95: LKPLAQSHAT), G (residues 100−118: PIKYLEFISEAIIHVLHSR), and the C-terminal portion of helix H (residues 132−149: NKALELFRKDIAAKYKEL). Only this portion of helix H was used, so that the results could be compared to an earlier study on the same system (Soman et al., 1991). Initial coordinates were taken from the X-ray crystal structure (Phillips, 1980), and acyl and methylamine blocking groups were added. In the simulations, protonation states were chosen to represent conditions near pH 7; in particular, glutamic and aspartic acids were negatively charged, lysine and arginine were positively charged, and all histidines were neutral. Each helical peptide was solvated in a preequilibrated, periodic parallelapiped box (49.6 Å by 24.8 Å by 24.8 Å) of 1024 water molecules. Any water molecules that overlapped with the peptide were removed. This left between 888 and 954 water molecules, depending on the peptide. The box was sufficiently large to ensure that the peptide was not influenced by neighboring peptide molecules. The solvated peptides were equilibrated for 15 ps at 298 K. Each equilibrated solvated peptide was used as the initial structure for two separate production simulations, one at 298 K and one at 368 K.

For each helical peptide, two simulations were run, at 298 K and at 368 K, each for between 700 and 1100 ps (helix A, 720 ps; helices E, G, and H, 1020 ps; helices B and F, 1080 ps). The primary purpose of these simulations was to compare the dynamics of the helical peptides at the control temperature (298 K) and at a moderately elevated temperature (368 K). Such a comparison allows us to assess the relative stabilities of the helices. At 298 K several of the helices appear to be equally stable; the moderately elevated temperature "encourages" the less stable of these to unfold, without the indiscriminate destruction of structure that would occur at very high temperatures (Daggett & Levitt, 1993).

The simulations all used the TIP3P model of water (Jorgensen et al., 1983) and the CHARMM, PARAM19 parameters to represent the protein, which are consistent with the TIP3P model (Brooks et al., 1983). A nonbonded cutoff of 9.25 Å was employed, using an atom−atom shifting function to minimize the effects of long-range force truncation for water−water interactions (Brooks et al., 1985). Atom-based Verlet lists were constructed every 25 time steps to process the nonbonded interactions based on a 9.75 Å list cutoff distance (Verlet, 1967). Minimum image periodic boundaries and a time step of 1.5 fs were used. The SHAKE constraint algorithm kept the protein hydrogen−heavy atom bonds and the geometry of all water molecules fixed (Mertz et al., 1991; Ryckaert et al., 1977). The calculations were performed using an optimized version of the CHARMM code, run in parallel processing mode on a CRAY Y-MP C90 (Brooks et al., 1983; Mertz et al., 1991). Each simulation took approximately 60 h of cpu time.

RESULTS

An overview of the helical stability of the peptides we studied is given in Figures 2 and 3. Figure 2 shows the time evolution of the $i, i + 4$ carbonyl O atom−amide H atom distances for helices A, B, E, F, G, and H, all at 368 K. The corresponding plots (data not shown) at 298 K show that all the helices except helix F are stable, with only the final C-terminal hydrogen bond distance showing any increase. Helices A, G, and H all appear to be relatively stable at 368 K. The C-terminus of helix A unwinds over the first half of the simulation and then re-forms in the latter half. Helices G and H also show some fraying at the C-terminus, but to a lesser extent. Helix B shows greater unwinding of the C-terminus, in the last 100−200 ps of the simulation, with some suggestion prior to that of the N-terminus unwinding. Some interesting features are found in the simulation of helix E at 368 K. The helix structure is immediately disrupted at two separate locations along the sequence. The unwinding of helix E continues throughout the entire simulation, expanding from the two initial sites, to an almost completely extended state after 1000 ps. Helix F also unwound at 368 K, as expected.

The features present in Figure 2 are consistent with the structures shown in Figure 3. Structures of the helices at 368 K are shown after 60 ps and at the end of the simulations (720 ps for helix A; 1020 ps for the helices E, G, and H; 1080 ps for helices B and F). Structures at 60 and 1020 ps are also shown for helix H at 298 K to demonstrate the stability of the helix at 298 K. The unwinding and rewinding of the C-terminus of helix A are evident, as are the unwinding of the C-terminus of helix B, the unfolding of helices E and

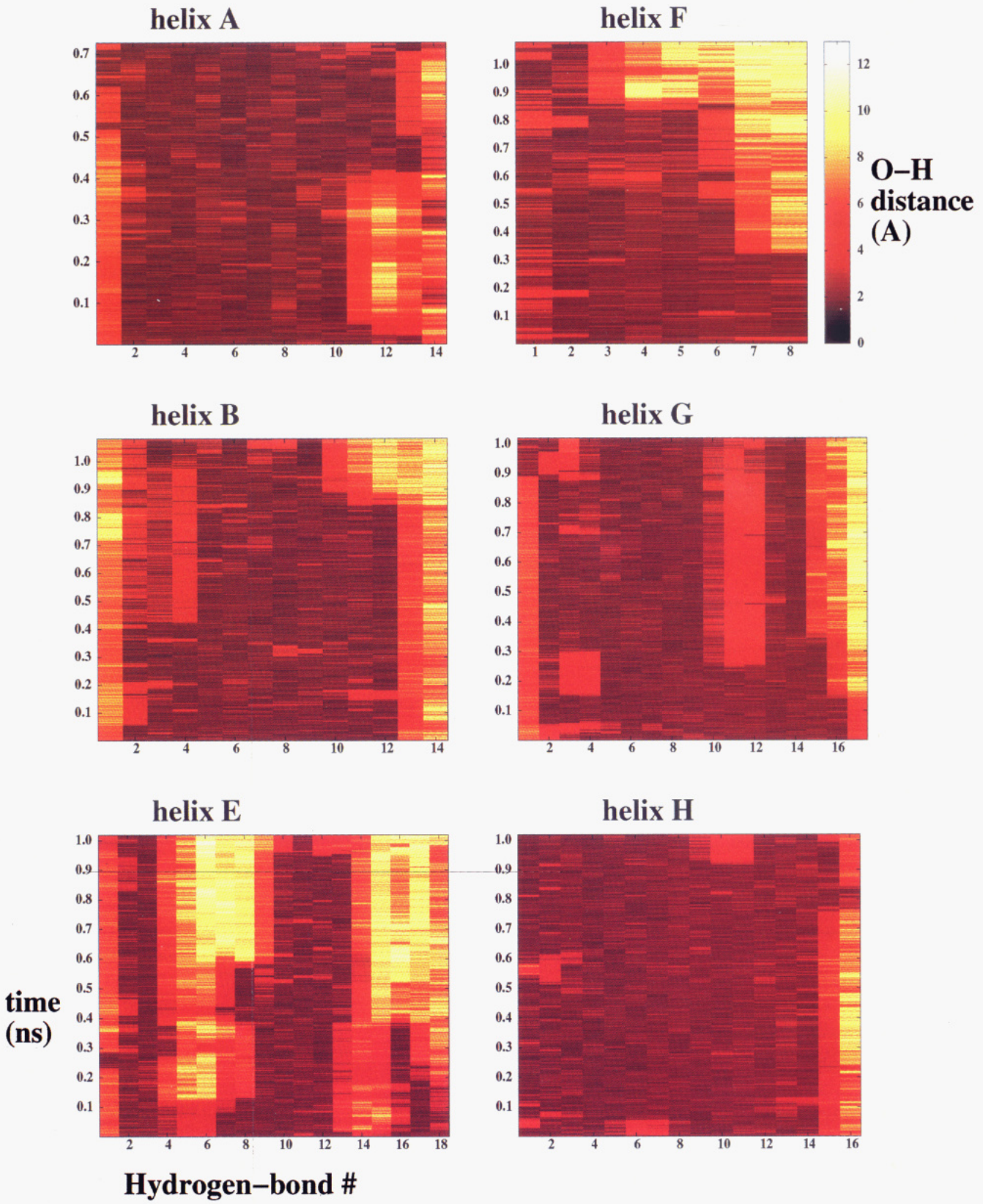

FIGURE 2: Time evolution of the i, $i + 4$ hydrogen bond distances for the simulations of helices A, B, E, F, G, and H all at 368 K. The carbonyl O atom−amide H atom distances (in angstroms) are color-coded.

F, and the relative stability of helices G and H. Intermediate structures are shown for helices E and H. The intermediate structure of helix E (after 540 ps) shows that a central portion of helix E remains intact, while unfolding has been initiated at two separate sites. The intermediate structure of helix H (after 900 ps) shows that helix H is well formed throughout most of the simulation and only kinks in the last 100 ps.

Table 1 shows, for each helix, the fraction of intact α-helical hydrogen bonds (defined by the i, $i + 4$ oxygen−hydrogen distance <2.5 Å), normalized by the number of residues in the helix, over the entire 368 K simulation and over the final 10% of the simulations at 368 K. Considering the complete trajectories at 368 K, the order of helix stability is H > A > G > B > F > E; considering the final 10%, the

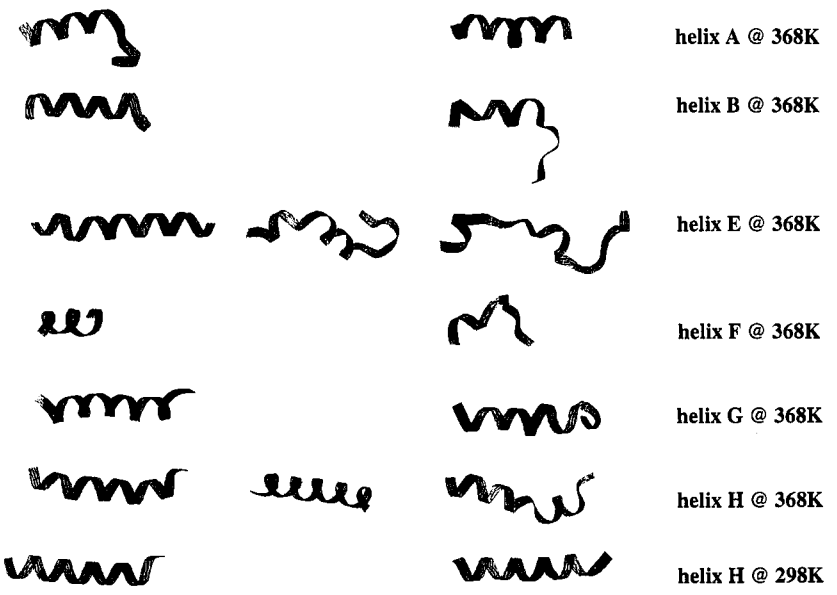

FIGURE 3: Structures from early (60 ps), intermediate (only for helices E and H), and late (720 ps for helix A; 1020 ps for helices E, G, and H; 1080 ps for helices B and F) in the trajectories simulated at 368 K and also for helix H at 298 K.

Table 1: Fraction of Intact α-Helical Hydrogen Bonds and Helicity of Each Helix during the Entire 368 K Simulations and during the Final 10% of the Simulation[a]

	fraction of intact helical hydrogen bonds		helicity	
helix	during total simulation	during final 10%	during total simulation	during final 10%
A	0.58	0.61	0.49	0.59
B	0.49	0.37	0.41	0.16
E	0.30	0.16	0.24	0.14
F	0.47	0.13	0.30	0.11
G	0.54	0.45	0.44	0.35
H	0.69	0.62	0.62	0.48

[a] Helicity is based on the values of the dihedral angles.

ordering is A > H > G > B > E > F. The changes in ordering reflect the refolding of helix A late in the simulation and the greater unfolding of helix F. These results combined with the 298 K simulations, in which only helix F was seen to be unstable, suggest the following ordering: H ≈ G ≈ A > B > E > F. A definition of helicity based on the dihedral angles lying close to certain "helical" values [as given in Hirst and Brooks (1994)] and requiring a helix to comprise at least three contiguous residues, leads to a picture similar to that given by the hydrogen-bonding analysis (Table 1).

The relative stabilities of the helices can be partly rationalized on the basis of the sequences of the helices. The more stable helices have patterns of hydrophobic residues that form i, $i + 4$ interactions that reinforce the helical structure. Helix A has a strongly hydrophobic side, comprising residues Trp7, Leu9, Val10, Leu11, Val13, Trp14, and Val 17, and a clear hydrophilic side: Gln8, His12, and Lys16. A similar distribution is seen for helix H, with the hydrophobic residues Leu135, Leu137, Phe138, Ile142, and Tyr146 on one side of helix H and several lysines (Lys133, Lys140, and Lys147) on the other. Helix G is strongly amphipathic, with Leu104, Ile107, Ile111, Ile112, Val114, and Leu115 on the hydrophobic face and Lys102, Glu105, Glu109, His113, and His116 on the hydrophilic face. Helix B is also amphipathic, with a hydrophobic face defined by Ile28, Val29, Ile30, Leu32, and Phe33 and a hydrophilic face defined by Asp20, His24, Asp27, and Arg31.

While helices A, B, G, and H are fairly similar in their amphipathic character, helix E is much less amphipathic. Helix F contains a proline and a histidine, which are both known to disfavor helical conformations. In holomyoglobin, there is a strong interaction between the histidine in helix F and the heme group. While both helices E and F undergo extensive unfolding in the 368 K simulations, we focus in more detail on the unfolding of helix E, which has a number of interesting aspects.

The unfolding of helix E follows mechanisms observed in other simulations of helix unfolding (DiCapua et al., 1991; Tobias & Brooks, 1991; Tirado-Rives & Jorgensen, 1991; Soman et al., 1991; Daggett & Levitt, 1992). In particular, we have observed the formation of i, $i + 3$ hydrogen-bonded intermediates. Figure 4 shows two examples of an i, $i + 4$ hydrogen bond being replaced by an i, $i + 3$ hydrogen bond in the partial unfolding of helix E. For clarity only the first 500 ps of the simulation are shown. In the 368 K simulation of helix E, the residue His64 plays an important role. In the native crystal structure, the distal His64 is coordinated to the iron ion, perpendicular to the plane of the heme group. The iron−His64 distance is 4.58 Å. While not covalently bonded at this distance, the loss of this interaction may destabilize helix E. Secondary structure prediction methods (Holley & Karplus, 1989; Garnier et al., 1978) suggest that intrinsically His64 does not have a strong tendency to be in a helix: both methods predict that His64 is not helical. Hargrove et al. (1994) concluded from mutation studies that His64 destabilizes the protein compared to other residues substituted into this site but that it is required to increase the affinity for oxygen and to inhibit autoxidation. There is a weaker suggestion that the other residue in helix E which has very large fluctuations at 368K, Gly73, also has a low tendency to be in a helix.

Unfolding of helix E is initiated at two separate locations in the helix. The unfolding of the C-terminal portion may be driven by the loss of the His64−iron interaction and also by the presence of a neighboring glycine, Gly65—glycine favors coil conformations over helical ones more than other residues because of its greater conformational entropy in the coil state (Lyu et al., 1990). The unfolding of the N-terminal

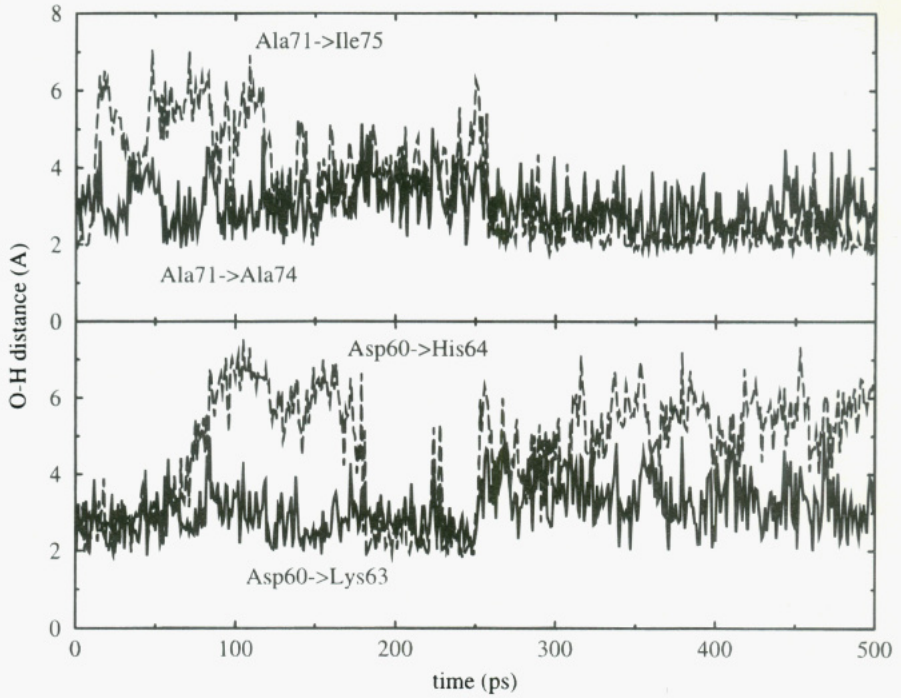

FIGURE 4: Two examples of an i, $i + 4$ hydrogen bond (dashed line) being replaced by an i, $i + 3$ hydrogen bond (solid line).

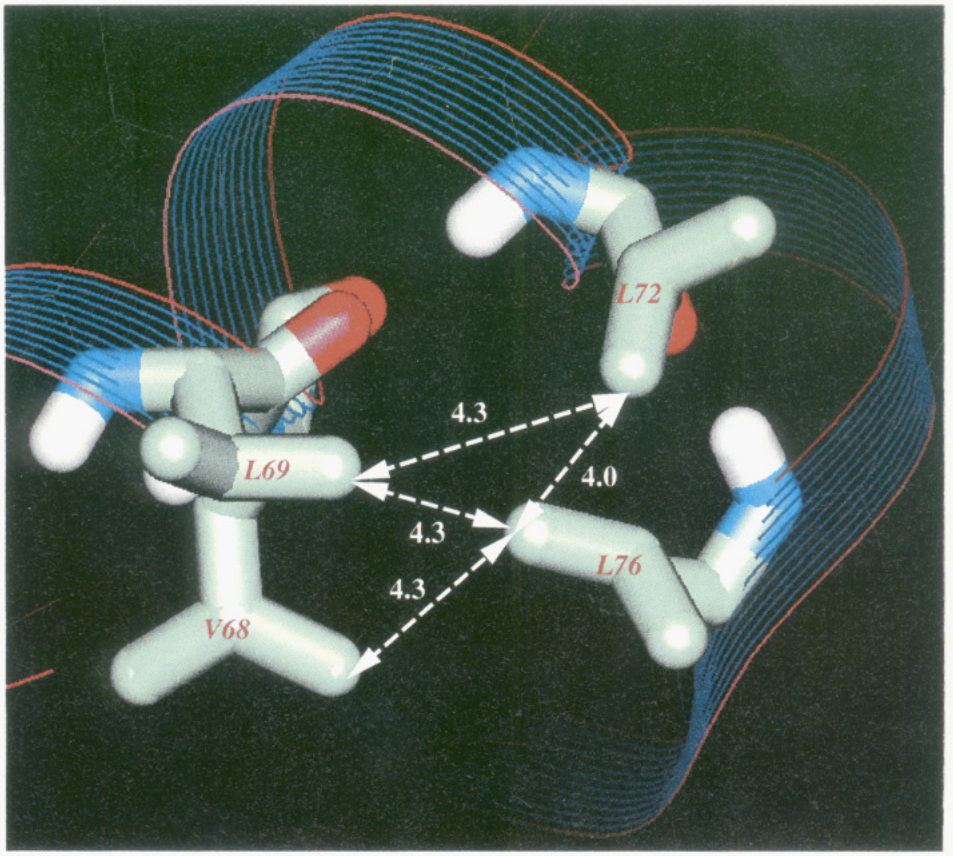

FIGURE 5: Transient hydrophobic cluster formed after 360 ps at the C-terminus of helix E during unfolding in the simulation at 368 K.

end appears to involve the formation of a cluster of interactions between hydrophobic residues. The side-chain−side-chain distances for several pairs of hydrophobic residues are below 5 Å for a considerable portion of the simulation. Figure 5 shows a transient hydrophobic cluster that formed after 360 ps. Leu76 forms two contacts with Val68 and Leu69, which disrupts the C-terminal helical structure. The suggestion is that, in the absence of hydrophobic interactions with the rest of the protein, the hydrophobic residues of helix E stabilize themselves by forming a hydrophobic cluster which destroys the helical structure.

We have examined the correlation of the stability of the isolated helices of myoglobin with the structure of the partially folded apomyoglobin intermediate at pH 4 (Hughson et al., 1990) and with the kinetic folding pathway of this intermediate (Jennings & Wright, 1993). Table 2 shows

Table 2: Relationship between the Stability of the Isolated Helices and the Structure and Kinetics of Refolding of the Apo Intermediate

residue (helix position)	calcd PFs of isolated helices at 368 K	time to achieve full protection on refolding	measured PFs of apo form at pH 4
V66 (E9)	1.0	S (≈2.5 s)	1
I75 (E18)	1.0	S	1
A74 (E17)	1.0	S	0.8
H64 (E7)	1.2	S	
E18 (A16)	1.2	M (≈1 s)	10
K77 (E20)	1.3	S	1
H113 (G14)	1.3	F (<5 ms)	
L76 (E19)	1.3	S	
V114 (G15)	1.4	F	30
V68 (E11)	1.4	S	0.4
V17 (A15)	1.7	F	40
L69 (E12)	2.0	S	1
I112 (G13)	2.7	F	80
F33 (B14)	3.0	F	5
K34 (B15)	3.6	S	0.9
L104 (G5)	5.0	F	8
L75 (E15)	6.6	S	0.4
T70 (E13)	7.1	S	2
W14 (A12)	8.2	F	20
I30 (B11)	8.9	F	10
I28 (B9)	10.6	M	2
A143 (H20)	11.4	F	20
R31 (B12)	12.0	M	2
I107 (G8)	12.0	F	40
V10 (A8)	12.9	F	200
L115 (G16)	14.7	F	7
L11 (A9)	15.6	F	60
I142 (H19)	24.8	F	60
A110 (G11)	25.3	F	7
L9 (A7)	30.5	F	90
F138 (H15)	32.2	F	10

protection factors (PFs) calculated from our simulations of the isolated helices at 368 K, the kinetic data of Jennings and Wright (1993), and the measured PFs of apomyoglobin at pH 4 (Hughson et al., 1990). Results are presented only for those residues for which there is some experimental data, although PFs have been calculated for all residues. The PFs are calculated from our simulation results using (Shalongo et al., 1994)

$$PF = 1/(1 - f_{HB}) \quad (1)$$

where f_{HB}, the fraction of time that the hydrogen bond is formed, is calculated directly from the simulation. A hydrogen bond was deemed to be formed if the carbonyl O−amide H distance was within 2.5 Å. The distances were taken from the production simulations of 720 ps for helix A, 1020 ps for helices E, G, and H, and 1080 ps for helices B and F.

One would not expect the stability of the isolated helices to be the only important influence on the kinetics and structure of the apomyoglobin intermediate at pH 4, and this is borne out in our data. Nevertheless, the stability of the isolated helices could play an important role. The correlation between the calculated PFs and the measured PFs is noticeable, given the differences between the experimental and theoretical systems. The trend for residues with high PFs (calculated or experimental) to achieve full protection quickly on refolding is also apparent.

Despite a general level of good agreement, some differences are apparent. The discrepancy between the calculated and measured PFs of residues Val17 and Glu18 at the end of helix A is most likely due to the formation of hydrogen bonds between the end of helix A and the beginning of helix B in the intact protein, and so the calculated PFs are too low because these interactions are lost in the isolated helices. The other most noticeable discrepancy is for residues Val114 and Ile112 in helix G. In the crystal structure of holomyoglobin, Val114 makes a number of interactions with residues in helix B and Ile112 makes a number of interactions with residues in helix H. Thus, the suggestion from our simulations is that these interactions may be present in some form in the apomyoglobin intermediate.

Another qualitative measure of the relative stabilities of the α-helical hydrogen bonds may be obtained from the quasiharmonic approximation:

$$(1/2)k_B T = (1/2)k_H\langle \Delta X^2 \rangle \quad (2)$$

where k_B is the Boltzmann constant, T is the temperature, k_H is the effective force constant of the hydrogen bond, and $<\Delta X^2>$ is given by

$$\langle \Delta X^2 \rangle = \frac{1}{N}\sum_{t=1}^{N}(x_t - \bar{x})^2 \quad (3)$$

where x_t is the i, $i + 4$ carbonyl O atom−amide H atom distance at time step t and N is the number of time steps. To examine this measure of relative stability, distances were computed for every hundredth time step in the production simulations, giving $N = 4800$ for helix A, $N = 6800$ for helices E, G, and H, and $N = 7200$ for helices B and F. The calculated force constants are shown in Figure 6 for the simulations at 298 K and at 368 K. The force constants are lower at 368 K than at 298 K, with a few exceptions. The more stable helices, A, G, and H, show less of a reduction in the effective hydrogen bond force constants at high temperature, whereas the peptides corresponding to helices B, E, and F show much larger reductions, consistent with the unfolding of the helices at the higher temperature. Another interesting feature of the figure is that hydrogen bonds in the centers of helices appear to have higher force constants, i.e., are more stable, than terminal hydrogen bonds. A similar result was noted by Shalongo et al. (1994) in their study of the model peptide acetyl(AAQAA)$_3$amide.

DISCUSSION

Hydrogen-exchange pulse labeling and stopped-flow circular dichroism experiments (Jennings & Wright, 1993) suggest that the dominant folding pathway of apomyoglobin is **unfolded → A·G·H → A·B·G·H → A·B·C·CD·D·E·G·H → native**. While helix H can form in isolation and may be considered to be an autonomous folding unit (Waltho et al., 1993), the G·H helical hairpin is not independently stable (Shin et al., 1993b). Thus, Jennings and Wright (1993) concluded that the folding of the A·G·H intermediate is probably due to both intrinsic helix stability and interactions between helices.

Previous simulations of apomyoglobin indicate that helix F is relatively unstable (Brooks, 1992; Tirado-Rives & Jorgensen, 1993). Analysis of the simulations of the isolated helices has allowed us to further investigate potential early events in the folding pathway of apomyoglobin. A comparison of the fluctuations at 368 K and at 298 K using the

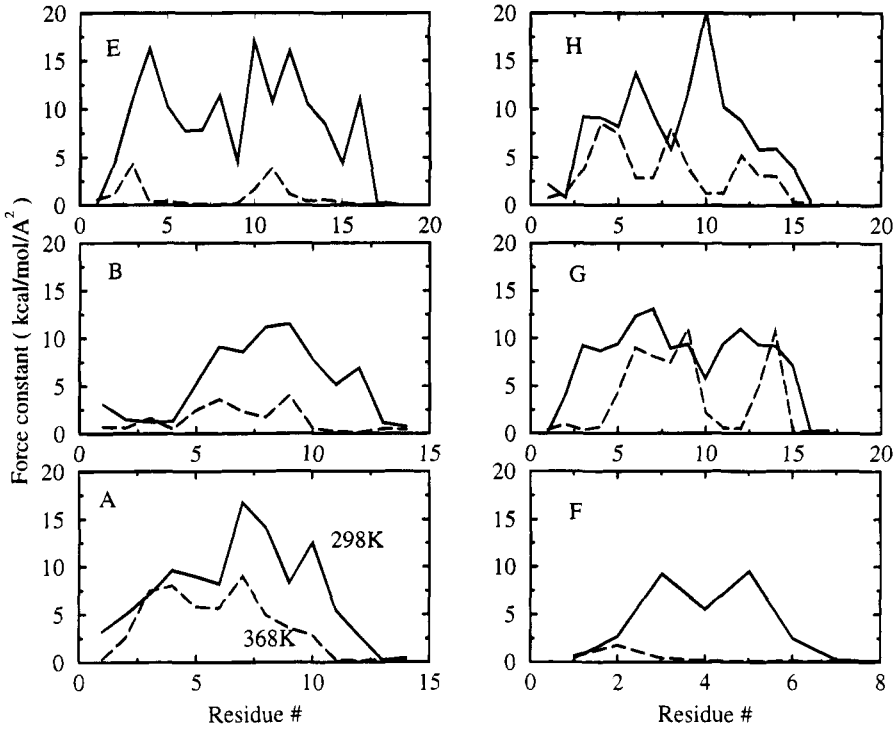

FIGURE 6: *i*, *i* + 4 hydrogen bond force constants calculated from the simulations using the quasiharmonic approximation.

quasiharmonic approximation and examination of hydrogen protection factors during the simulations clearly suggest the following order of stability, **helices A, G, and H (most stable) > B > E > F (least stable)**, in basic agreement with the experimental data (Hughson et al., 1990; Barrick & Baldwin, 1993; Jennings & Wright, 1993). The stability of helices A, G, and H arises, in part, from a number of *i*, *i* + 4 interactions between hydrophobic residues in the peptides, which reinforce the helical structure. Also consistent with the data of Jennings and Wright (1993) is the suggestion from our simulations that the C-terminus of helix G may be stabilized by contacts with part of helix B. In particular, our simulations show that the region around residues Ile112, His113, and Val114 in helix G is destabilized in the isolated peptide (Table 1), which suggests that the interactions seen in the crystal structure of holomyoglogin (Phillips, 1980) between Arg31 and His113 and between Ile28 and Val114 may have a role in stabilizing an early folding intermediate. The experimental observation that the N-terminus of helix H has low helical propensity suggests that contacts between helix A and the N-terminus of helix H may provide another stabilizing interhelical interaction.

The consensus picture of the folding pathway of apomyoglobin that emerges from simulation and experiment is one in which regions with high intrinsic helical propensity, corresponding to helices A, G, H, and to a lesser extent helix B, form early, along with the turn region between helices G and H. These fragments of secondary structure coalesce to form an intermediate, comprising helices A, G, H, and part of B, that has been isolated and characterized at pH 4 (Hughson et al., 1990). Folding continues with the formation of helix E and the rest of helix B. The relative intrinsic stabilities of the helices estimated from our simulations strongly correlate with this pathway, and thus the influence of intrinsic helical propensity appears to play a significant role in the folding of apomyoglobin.

ACKNOWLEDGMENT

Computational resources from the NSF Meta Center Allocation Program, the Cray Research Corporation, and the Pittsburgh Supercomputing Center are acknowledged.

REFERENCES

Barrick, D., & Baldwin, R. L. (1993) *Biochemistry 32*, 3790−3796.
Barrick, D., Hughson, F. M., & Baldwin, R. L. (1994) *J. Mol. Biol. 237*, 588−601.
Brooks, C. L. (1992) *J. Mol. Biol. 227*, 375−380.
Brooks, C. L., Pettitt, B. M., & Karplus, M. (1985) *J. Chem. Phys. 83*, 5898−5908.
Cocco, M. J., Kao, H.-Y., Phillips, A. T., & Lecomte, J. T. J. (1992) *Biochemistry 31*, 6481−6491.
Creighton, T. E. (1992) *Protein Folding*, Freeman & Co., New York.
Daggett, V., & Levitt, M. (1992) *J. Mol. Biol. 223*, 1121−1138.
Daggett, V., & Levitt, M. (1993) *J. Mol. Biol. 232*, 600−619.
DiCapua, F. M., Swaminathan, S., & Beveridge, D. L. (1991) *J. Am. Chem. Soc. 113*, 6145−6155.
Dyson, H. J., Merutka, G., Waltho, J. P., Lerner, R. A., & Wright, P. E. (1992a) *J. Mol. Biol. 226*, 795−817.
Dyson, H. J., Sayre, J. R., Merutka, G., Shin, H.-C., Lerner, R. A., & Wright, P. E. (1992b) *J. Mol. Biol. 226*, 819−835.
Garnier, J., Osguthorpe, D. J., & Robson, B. (1978) *J. Mol. Biol. 120*, 97−120.
Griko, Y. V., & Privalov, P. L. (1994) *J. Mol. Biol. 235*, 1318−1325.
Griko, Y. V., Privalov, P. L., Venyaminov, S. Y., & Kutyshenko, V. P. (1988) *J. Mol. Biol. 202*, 127−138.
Hargrove, M. S., Kryzwda, S., Wilkinson, A. J., Dou, Y., Ikeda-Saito, M., & Olson, J. S. (1994) *Biochemistry 33*, 11767−11775.
Hirst, J. D., & Brooks, C. L. (1994) *J. Mol. Biol. 243*, 143−148.
Holley, L. H., & Karplus, M. (1989) *Proc. Natl. Acad. Sci. U.S.A. 86*, 152−156.
Hughson, F. M., Wright, P. E., & Baldwin, R. L. (1990) *Science 249*, 1544−1548.
Jennings, P. A., & Wright, P. E. (1993) *Science 262*, 892−896.
Jorgensen, W. L., Chandrasekhar, J., Madura, J., & Klein, M. L. (1983) *J. Chem. Phys. 79*, 926−935.
Kraulis, P. J. (1991) *J. Appl. Crystallogr. 24*, 946−950.

Lyu, P. C., Liff, M. I., Marky, L. A., & Kallenbach, N. R. (1990) *Science 250*, 669−673.
Mertz, J. E., Tobias, D. J., Brooks C. L., & Singh, U. C. (1991) *J. Comput. Chem. 12*, 1270−1277.
Nishii, I., Kataoka, M., Tokunaga, F., & Goto, Y. (1994) *Biochemistry 33*, 4903−4909.
Phillips, S. V. E. (1980) *J. Mol. Biol. 142*, 531−554.
Ryckaert, J.-P., Ciccotti, G., & Berendsen, H. J. C. (1977) *J. Comput. Phys. 23*, 327−341.
Shalongo, W., Dugad, L., & Stellwagen, E. (1994) *J. Am. Chem. Soc. 116*, 8288−8293.
Shin, H.-C., Merutka, G., Waltho, J. P., Wright, P. E., & Dyson, H. J. (1993a) *Biochemistry 32*, 6348−6355.
Shin, H.-C., Merutka, G., Waltho, J. P., Wright, P. E., & Dyson, H. J. (1993b) *Biochemistry 32*, 6356−6364.
Soman, K. V., Karimi, A., & Case, D. A. (1991) *Biopolymers 31*, 1351−1361.
Tirado-Rives, J., & Jorgensen, W. L. (1991) *Biochemistry 30*, 3864−3871.
Tirado-Rives, J., & Jorgensen, W. L. (1993) *Biochemistry 32*, 4175−4184.
Tobias, D. J., & Brooks, C. L. (1991) *Biochemistry 30*, 6059−6070.
Verlet, L. (1967) *Phys. Rev. 159*, 98−103.
Waltho, J. P., Feher, V. A., Lerner, R. A., & Wright, P. E. (1989) *FEBS Lett. 250*, 400−404.
Waltho, J. P., Feher, V. A., Merutka, G., Dyson, H. J., & Wright, P. E. (1993) *Biochemistry 32*, 6337−6347.
Yang, A.-S., & Honig, B. (1994) *J. Mol. Biol. 237*, 602−614.

BI942948+